On the Use of a Directly Modulated Laser in a Phase Modulated-Assisted mmW Signal Generation and Transmission Link

M. Botella-Campos, J. Mora, and B. Ortega, *Senior Member, IEEE*

***Abstract*—We propose and experimentally demonstrate the use of a directly modulated laser (DML) in an optical phase modulated (PM)-assisted millimeter-wave (mmW) signal generation system. A comprehensive analytical model is provided to accurately describe the system frequency response, which is also validated by the experimental measurements. For the purpose of the system characterization, the transmission performance is analyzed using a QPSK signal at different operating mmW frequencies over large received optical power (RoP) and electrical data power ranges in a 10 km standard single mode fiber (SSMF) link. Both the impact of the noise and the DML nonlinearities lead to identify the optimal conditions for the system operation where PM-based mmW signal photonic generation demonstrates total transparency with no further signal degradation. Final comparison with IM technique for mmW signal generation leads to assess the robustness of PM solution which makes it promising for the deployment of future communication networks.**

***Index Terms*—5G-6G mobile communications, directly modulated lasers, microwave photonics, millimeter-wave signal generation, phase modulation, radio-over-fiber.**

I. Introduction

WHILE the fifth generation (5G) mobile communications networks is currently deployed throughout the world, academy and industry focus their goals to satisfy the future demands for sixth generation (6G) systems, which are not only based on the exponential growth of mobile traffic and mobile subscriptions but also on new disruptive services and applications. Accordingly, key enabling technologies for 6G can be categorized into these groups [1]: new spectrum, new networking, new air interface, new architecture, and new paradigm; which are also driven by the intrinsic need of mobile communication society to continuously improve the cost, energy, and spectrum efficiency.

Manuscript received 5 May 2023; revised 14 July 2023; accepted 27 July 2023. Date of publication 1 August 2023; date of current version 16 December 2023. This work was supported in part by OPTIMISE through MCIN/AEI/10.13039/501100011033 under Grant PID2021-126514OB-I00, in part by ERDF A way of making Europe, and in part by Generalitat Valenciana under Project PROMETEO 2021/015. *(Corresponding author: M. Botella-Campos.)*

The authors are with the Instituto de Telecomunicaciones y Aplicaciones Multimedia, ITEAM, Universitat Politècnica de València, 46022 Valencia, Spain (e-mail: marbocam@teleco.upv.es; jmalmer@iteam.upv.es; bortega@dcom.upv.es).

More concretely, the main new spectrum enablers consist of using millimeter wave (mmW) and terahertz (THz) bands, visible light communications (VLC), optical wireless communications (OWC), and dynamic spectrum management (DSM).

The mmW technology, namely employing 30 to 300 GHz spectral range, was already introduced by the 5G new radio, but remains as an essential component in future 6G networks due to its broad bandwidth compared to legacy RF technologies working below 6 GHz, the smaller antenna size (i.e., larger dimension of antenna arrays), the use of low attenuation bands (i.e., 35 GHz) for long-distance peer-to-peer communications, and the possibility of exploitation of frequencies suffering high attenuation (i.e., 60 GHz) by short links with stringent safety requirements. However, there are still some challenges to overcome such as the blockage in line-of-sight (LOS) scenarios with presence of multiple moving objects, the interference among different access points in scenarios with dense links and the broad bandwidth and high transmission power that can lead to severe non-linear signal distortions and imposes higher technical requirements for the electronics than those for RF devices [2].

Standard single-mode fibers (SSMF) offer low loss propagation and distribution of mmW signals over long distances in Radio-over-Fiber (RoF) networks. Additionally, the literature presents many promising photonic approaches for mmW signal generation, such as those based on the use of external modulators, that results attractive due to the simplicity and high purity generated signals [3]. Despite the numerous optical heterodyning approaches presented in the literature based on intensity modulation, the use of phase modulators (PM) has been widely reported as an attractive approach to avoid the lack of thermal stability of those ones using Mach–Zehnder modulator (MZM) which is related to the biasing drift. Additionally, proper biasing of a MZM is an important drawback for photonic subcarrier frequency up-converters which require an efficient optical carrier suppression. Moreover, commercial MZMs have asymmetric arms due to manufacturing limitation which further reduces the optimization of the required biasing point. Indeed, previous works present the mmW signals generation by a null-biased MZM but an external RF hybrid is required to achieve an effective suppression of the optical carrier [4]. In general, PM-based approaches usually show higher signal-to-noise ratio than IM schemes since the insertion losses are lower in the former case.

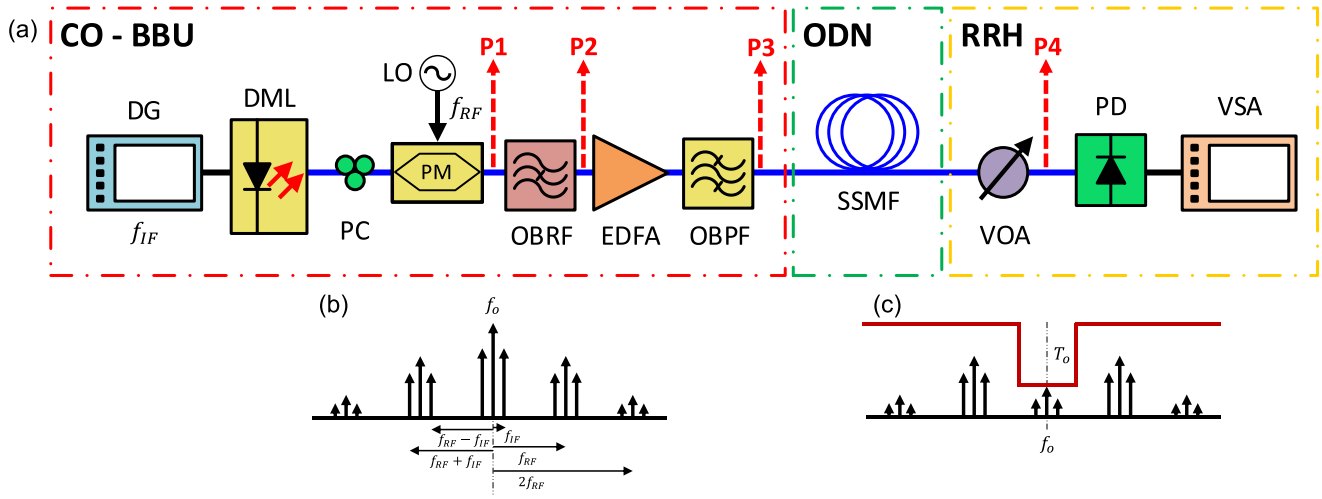

Fig. 1. (a) Schematic for DML signal transmission over PM-based mmW generated signal with optical carrier filtering, (b) Optical spectrum after the PM (P1) and (c) Optical spectrum after the fiber link just prior to PD (P4). CO-BBU: baseband unit at the central office, DG: digital generator, DML: directly modulated laser, PC: polarization controller, PM: phase modulator, LO: local oscillator, OBRF: optical band-rejection filter, EDFA: erbium doped amplifier, OBPF: optical bandpass filter, ODN: optical distribution network, SSMF: standard single mode fiber, RRH: remote radio head, VOA: variable optical attenuator, PD: photodetector, VSA: vector signal analyzer.

In this context, the lack of any dc-bias signal can be considered one of the main advantages of the optical phase modulators although phase-to-intensity modulation (PM-to-IM) conversion is needed before photodetection. This can be done by signal propagation over a dispersive device, i.e., fiber chromatic dispersion [5] although the fiber length must be carefully chosen to optimize the system performance. Alternatively, this PM-to-IM conversion can be performed by selecting the appropriate optical bands to obtain the desired mmW frequency after opto-electronic conversion by means of fixed optical filters such as fiber Bragg gratings [6] or other sophisticated filtering devices [7]. In addition, nonlinear effects are used for narrowband filtering by means of Brillouin assisted fiber rings [8] or remote injection locking schemes in distributed feedback laser diode (DFB LD) [9].

Moreover, the interest of PM as a component in the optical transceiver has been recently shown in experimental demonstrations, such as bidirectional fiber-wireless systems using PM for uplink [10], [11], or both downlink and uplink [12]. Recently, M-quadrature amplitude modulation (QAM) vector mmW signal generation has been experimentally demonstrated employing a frequency doubling scheme and a precoding technique [13], [14]. However, so far, the data signal carried at RF drives the phase external modulator which requires specific electronic drivers and lacks from the advantages of directly modulated laser (DML)-based approach already proposed for the implementation of future cloud-radio access networks (C-RAN) including photonic mmW generation based on MZM [15].

In this article, to the best of our knowledge, we present, for the first time, an approach based on intensity modulation for data transmission by means of a DML in photonically generated mmW signals using optical filtering to achieve PM-to-IM frequency up-conversion. The system performance is analyzed both theoretically and experimentally in order to optimize properly the transmission of the generated mmW signal.

The article is structured as follows. Section II provides the theoretical and experimental system description, Section III presents the experimental transmission results, also including a comparison with IM scheme for the sake of final assessment of the proposed approach, and Section IV summarizes the main conclusions of this work.

II. System Description

A. Analytical Model

In this section, we present the theoretical analysis of a new architecture for photonic mmW signal generation based on external PM frequency up-conversion and directly intensity modulation for data transmission, as depicted in Fig. 1(a).

A DML located at the baseband unit (BBU) in the central office (CO) emits an optical carrier at an angular optical frequency $\omega_0 = 2\pi f_o$ which is modulated by data carried by an intermediate frequency ω_{IF}. The digital data sequence is provided by a data generator (DG) with an electrical power P_{IF}.

In the following, and for the sake of characterizing the system response, the optical field at the DML output is analytically derived after laser direct modulation by a single tone at an angular frequency $\omega_{IF} = 2\pi f_{IF}$. Provided small-signal regime is considered, the following expression is obtained [15], [16]:

$$E_{DML}\ (t) = \sqrt{P_o} e^{j\omega_o t}\ \left[1 + m_+ \cdot e^{j\omega_{IF} t} + m_- \cdot e^{-j\omega_{IF} t}\right] \tag{1}$$

where P_o is the optical output power of the laser and the modulation indexes m_+ and m_- are given by:

$$m_+ = \frac{1}{2}\left(m_{AM} + jm_{PM}e^{j\Delta\varphi}\right)$$
$$m_- = \frac{1}{2}\left(m_{AM} + jm_{PM}e^{-j\Delta\varphi}\right) \quad (2)$$

Here, m_{PM} and m_{AM} are the phase and amplitude modulation indexes, respectively, and $\Delta\varphi$ is the phase difference between the phase and amplitude modulation introduced by the laser. Note that m_{AM} is directly proportional to $\sqrt{P_{IF}}$. All these parameters are related to the chirp characteristics of the laser, i.e., the linewidth enhancement factor, α, and the adiabatic laser chirp, κ. Concretely,

$$\frac{m_{PM}}{m_{AM}} \cdot e^{j\Delta\varphi} = \alpha\left(1 - j\frac{\kappa P_o}{\omega_{IF}}\right) \quad (3)$$

The output field $E_{DML}(t)$ is then sent into a polarization controller (PC) for optimizing its polarization state before launching onto a PM. This PM is driven by a single electrical tone with angular frequency $\omega_{RF} = 2\pi f_{RF}$ and power P_{RF}, generated by a local oscillator (LO). Thus, its impulse response can be written as follows:

$$h_{PM}(t) = e^{jm_{RF}cos(\omega_{RF}t)} = \sum_n (j)^n J_n(m_{RF})\, e^{jn\omega_{RF}t} \quad (4)$$

where m_{RF} is the modulation index which is related to the efficiency of the PM as the ratio between the applied voltage V_{RF} which is proportional to $\sqrt{P_{RF}}$ and the intrinsic half wave voltage V_π parameter. Since small signal regime is considered, the only relevant terms are n = 0, 1 and 2 in (4).

The resulting optical modulated signal, i.e., $E_{DML}(t) \cdot h_{PM}(t)$, is then sent to an optical band-rejection filter (OBRF) to suppress the optical carrier. Fig. 1(b) shows the optical spectra after PM where first and second order harmonic distortion correspond to f_{RF} and $2f_{RF}$, respectively. In this experiment, a rectangular optical filter $h_{OBRF}(\omega)$ is defined with a frequency transfer function:

$$h_{OBRF}(\omega) = \begin{array}{ll} T_o & \text{if } |\omega - \omega_o| < \frac{\delta\omega_o}{2} \\ 1 & \text{if } |\omega - \omega_o| > \frac{\delta\omega_o}{2} \end{array} \quad (5)$$

where $\delta\omega_o$ is the optical bandwidth of the filter and T_o is the nominal transmission at the rejected band. Note that $T_o = 1$ means there is no actual OBRF.

At the optical distribution network (ODN), the signal is then transmitted through a SSMF link to the remote radio head (RRH). Note that an erbium-doped fiber amplifier (EDFA) is included to compensate the optical losses and an optical band-pass filter (OBPF) is used to reduce the amplified spontaneous emission (ASE) noise. The impulse response of the SSMF, $h_{SSMF}(t)$, can be expressed as [17]:

$$h_{SSMF}(t) = \frac{1}{\sqrt{j2\pi\beta_2 L}}\, e^{j\frac{\pi}{2\beta_2 L}t^2} \quad (6)$$

where the dispersion parameter β_2 is the second derivative of the propagation constant with respect to the optical frequency at ω_0, and L is the fiber length.

In this way, the input electric field at the photodiode, $E_{PD}(t)$, in Fig. 1, is given by the convolution between the electric field after the modulation stages and the response of the dispersive section, given by:

$$E_{PD}(t) = [E_{DML}(t) \cdot h_{PM}(t)] \otimes h_{OBRF}(t) \otimes h_{SSMF}(t) \quad (7)$$

where $h_{OBRF}(t)$ is the time impulse response of the OBRF, given by the Fourier Transform of the frequency response in (5). In addition, a variable optical attenuator (VOA) is considered to control the received optical power (RoP) just before the photodetector (PD). Therefore, by using the abovementioned equations, the following expression can be obtained:

$$\begin{aligned} E_{PD}(t) = \Big[& T_o J_o(m_{RF}) + jJ_1(m_{RF})\, e^{j\frac{1}{2}\beta_2 L\omega_{RF}^2} \\ & \times \left(e^{j\omega_{RF}t} + e^{-j\omega_{RF}t}\right) \\ & - J_2(m_{RF})\, e^{j2\beta_2 L\omega_{RF}^2}\left(e^{j2\omega_{RF}t} + e^{-j2\omega_{RF}t}\right)\Big] e^{j\omega_o t} \\ & + T_o J_o(m_{RF})\, e^{j\frac{1}{2}\beta_2 L\omega_{IF}^2}\left(m_+ \cdot e^{j\omega_{IF}t} + m_- \right. \\ & \left. \cdot\, e^{-j\omega_{IF}t}\right) e^{j\omega_o t} + jJ_1(m_{RF})\, e^{j\frac{1}{2}\beta_2 L(\omega_{RF}+\omega_{IF})^2} \\ & \times \quad m_+ e^{j(\omega_{RF}+\omega_{IF})t} + m_- e^{-j(\omega_{RF}+\omega_{IF})t}\Big) e^{j\omega_o t} \\ & + jJ_1(m_{RF})\, e^{j\frac{1}{2}\beta_2 L(\omega_{RF}-\omega_{IF})^2} \\ & \times \quad m_- \cdot e^{j(\omega_{RF}-\omega_{IF})t} + m_+ \cdot e^{-j(\omega_{RF}-\omega_{IF})t}\Big) e^{j\omega_o t} \\ & - J_2(m_{RF})\, e^{j\frac{1}{2}\beta_2 L(2\omega_{RF}+\omega_{IF})^2} \\ & \times \quad m_+ \cdot e^{j(2\omega_{RF}+\omega_{IF})t} + m_- \cdot e^{-j(2\omega_{RF}+\omega_{IF})t}\Big) \\ & \times e^{j\omega_o t} - J_2(m_{RF})\, e^{j\frac{1}{2}\beta_2 L(2\omega_{RF}-\omega_{IF})^2} \\ & \times \quad m_- \cdot e^{j(2\omega_{RF}-\omega_{IF})t} + m_+ \cdot e^{-j(2\omega_{RF}-\omega_{IF})t}\Big) e^{j\omega_o t} \end{aligned} \quad (8)$$

As shown in the optical spectrum in Fig. 1(c), the electrical field $E_{PD}(t)$ shows several bands at different optical frequencies $\omega_o \pm n\omega_{RF} \pm m\omega_{IF}$. Note that the optical carrier (ω_o) and the signal modulated bands located at $\omega_o \pm \omega_{IF}$ are minimized by means of the transmission T_o of the filter.

Consequently, the electrical current detected by the photodiode, $i(t)$, can be calculated as:

$$i(t) = \Re \cdot P(t) = \Re \cdot |E_{PD}(t)|^2 \quad (9)$$

where $P(t)$ is the RoP and $\Re$ is the photodiode responsivity.

When the photocurrent $i(t)$ is calculated in (9), different contributing terms are obtained at the electrical frequencies $n\omega_{RF} \pm m\omega_{IF}$. The bands of interest for the up-converted mmW signal are recovered at $\omega_{mmW} = 2\omega_{RF} \pm \omega_{IF}$ corresponding to the beating between different optical bands at the PD, i.e., $(\omega_o \pm \omega_{RF} \pm \omega_{IF})$ and $(\omega_o \pm \omega_{RF})$ although additional contributions are obtained from the beating of $(\omega_o \pm 2\omega_{RF})$ and $(\omega_o \pm \omega_{IF})$, and also from (ω_o) and $(\omega_o \pm 2\omega_{RF} \pm \omega_{IF})$ bands. Because of the contribution of the optical carrier (ω_o) and the modulated data $(\omega_o \pm \omega_{IF})$ terms are determined by the transmission T_o, when it tends to zero the higher-order PM terms are negligible and the recovered mmW signal is mainly given by the beating

TABLE I
ANALYTICAL TERMS OF THE PHOTOCURRENT AMPLITUDE AT mmW BAND

L	T_o	$i_{RF}(2\omega_{RF}-\omega_{IF})$	
0	1	0	(10)
L	1	$2\Re P_o \cdot m_{AM}\left(\frac{m_{RF}}{2}\right)^2 \cdot \sin^2\theta \cdot \left[\sqrt{1+\alpha^2}\cos(\theta - atan\alpha) + j\alpha\frac{\kappa P_o}{\omega_{IF}}\cdot\sin\theta\right]$	(11)
L	0	$\Re P_o \cdot m_{AM}\left(\frac{m_{RF}}{2}\right)^2 \cdot \left[\left[\sqrt{1+\alpha^2}\cos(\theta - atan\alpha) + j\alpha\frac{\kappa P_o}{\omega_{IF}}\cdot\sin\theta\right]\right]$	(12)

between $(\omega_o \pm \omega_{RF} \pm \omega_{IF})$ and $(\omega_o \pm \omega_{RF})$. Therefore, the filtering requirements are less demanding compared to previous schemes [6], [7] because the higher order terms do not contribute to the mmW signal so full signal suppression is not required. Finally, since the system response is similar at both upper and lower bands, the lower one is used along the manuscript to show the system performance without loss of generality.

After analytical derivations, simplified expressions can be obtained for $i_{RF}(2\omega_{RF}-\omega_{IF})$ in the cases of interest, as shown in Table I, where $\theta = \frac{1}{2}\beta_2 L\omega_{RF}(2\omega_{RF}-\omega_{IF})$. Theoretical results in (10) and (11) are obtained without OBRF, i.e., $T_o = 1$, for OB2B and over a SSMF link with a length of L, respectively, while (12) shows the response of the system including the ideal band rejection filter ($T_o = 0$) and the fiber link.

As expected, (10) leads to null signal at mmW frequency under OB2B scenario ($L = 0$ km) when no filter is considered. However, the transmission in (12) is equivalent to that obtained for IM-based up-conversion scheme reported in [16] although it is worth noting that this approach based on PM has significant advantages compared to the previous one, such as low insertion losses and the lack of biasing voltage, i.e., bias-drift-free modulator. However, note that an additional factor $(\sin^2\theta)$ appears in the first term of (11) which implies the suppression of the up-conversion at different mmW frequencies, f_{mmW}, due to dispersion effects, as can be calculated from the following expression:

$$f_{mmW} = 2f_{RF} - f_{IF} = \frac{n}{2\pi\beta_2 L f_{RF}} \quad n = 0, \pm 1 \tag{13}$$

Such factor comes from the beating between the optical carrier (ω_o) and the optical sidebands which are generated at the optical frequencies $\omega_o \pm (2\omega_{RF} - \omega_{IF})$. Note this contribution disappears when the notch filter is considered, i.e., $T_o = 0$, according to (12).

B. Experimental Setup

The DML (Emcore 5021T-D) output signal spectrum is centered at $\lambda_0 = 1547.69$ nm with an optical power of $P_o = 7.58$ dBm and a 3 dB modulation bandwidth of 4.85 GHz. The chirp characteristics of the DML, i.e., linewidth enhancement factor, α, and adiabatic laser chirp, κ, have a value of 2 and 13 GHz/mW, respectively. In this experiment, Rohde & Schwarz SMW200A was used for generating the modulation signal, i.e., a single tone at the electrical subcarrier $f_{IF} = 200$ MHz, that is applied to the DML with an electrical power $P_{IF} = 0$ dBm.

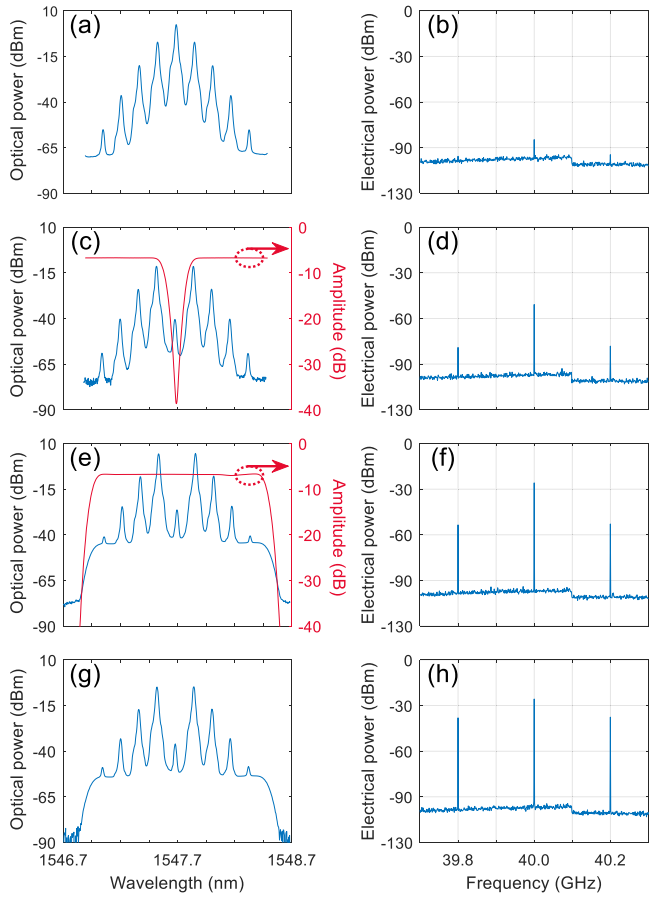

Fig. 2. Measured optical (left) and electrical (right) power spectra at different points in the schematic shown in Fig. 1: (a), (b) P1; (c), (d) P2; (e), (f) P3; and (g), (h) P4.

The phase modulation was performed using the Photline MPZ-LN-20-P-P-FC-FC PM with 2.2 dB insertion losses, a 3 dB bandwidth around 20 GHz and a half wave voltage $V_\pi = 7.4\,V$. It was driven by an electrical single tone, as LO signal, at $f_{RF} = 20$ GHz with a $P_{RF} = 23$ dBm which was generated by the instrument Agilent 8267C. Note that large PM efficiency can be achieved for producing mmW modulated signals because commercial PMs are available up to 40 GHz and the modulator is driven at frequencies around $f_{mmW}/2$. Fig. 2(a) and (b) present the optical and electrical spectra of the phase modulated signal at P1. Fig. 2(a) shows an extinction ratio (ER) between the optical carrier and optical sidebands close to 4.8 dB. Moreover, Fig. 2(b) displays the electrical photodetected signal after the PM where non up-converted mmW signal is present, as predicted in (10). This is because phase modulation needs to be converted into intensity modulation for signal recovery. Note that the mmW

bands of interest are centered at $f_{mmW} = 2f_{RF} \pm f_{IF}$, i.e., 39.8 and 40.2 GHz for the lower and upper bands, respectively.

A programmable optical processor (Finisar Waveshaper 4000 s) was used as an OBRF. In this experiment, a notch filter with a 3 dB bandwidth of 0.22 nm was reconfigured by means of the OBRF, as depicted in Fig. 2(c), with a transmission $T_o = 32$ dB and 6.7 dB insertion losses. Fig. 2(c) and (d) display the optical and electrical signal spectra, respectively, measured after OBRF at P2 in Fig. 1. Fig. 2(c) shows the optical power of the carrier decreases to -40.6 dBm while the optical sidebands power levels are -11.5 dBm, so ER $\sim$29.1 dB. Such optical filtering enables the intensity to phase conversion and mmW signal can now be recovered at 39.8 and 40.2 GHz, as depicted in Fig. 2(d). Note that photonic up-conversion is held after filtering the optical carrier in the phase modulated signal.

To compensate the optical losses, the optical signal is amplified by an EDFA (Amonics AEDFA-23-B-FA) with a fixed gain of 16.6 dB and filtered by an OBPF (Alnair BVF-100) to reduce the ASE noise. Here, the OBPF has a 3 dB bandwidth of 1.25 nm and 4.9 dB insertion losses. Next, Fig. 2(e) and (f) exhibit the optical and electrical spectra, respectively, measured at P3 in Fig. 1. In the former one, it can be observed that optical amplification and filtering lead to optical sidebands power level of 4.5 dBm with an ER = 30.9 dB.

Finally, Fig. 2(g) shows the signal spectrum after transmission over a 10 km long fiber link, i.e., at P4 in Fig. 1, with a dispersion parameter $\beta_2 = -22\, ps^2/km$. Fig. 2(h) depicts the corresponding electrical spectrum after optoelectronic conversion which was measured by a 50 GHz 3 dB bandwidth photodiode (Finisar XPDV3120R) working in a linear regime. The mmW signal is generated by the beating of both sidebands and the system performance is evaluated at a vector signal analyzer (VSA, Rohde & Schwarz FSW43). Additionally, the received optical power at the PD input is controlled by a VOA (Thorlabs EVOA1550A).

In the following, the theoretical model described above is validated by calculating and measuring the electrical system response at the mmW band ($f_{mmW} = 2f_{RF} - f_{IF}$) of the current amplitude after photodetection for an electrical power $P_{IF} = 0$ dBm and a constant RoP level of 3 dBm. Fig. 3 displays the frequency response of three experimental scenarios corresponding to the cases described in (10), (11) and (12). The system response was measured by varying the frequency of the single tone from $f_{IF} = 200$ MHz up to 20 GHz, with a fixed electrical power, P_{IF}, as modulating signal at the DML, while the electrical power was measured at the signal frequency of interest, $f_{mmW} = 2f_{RF} - f_{IF}$.

Firstly, we observe that the frequency response of the OB2B structure without a filter (i.e., $T_o = 1$) presented in Fig. 3 shows amplitude levels around -100 dBm, since pure phase modulation is applied [18]. However, significant differences are found in the frequency response when considering a 10 km SSMF link without the use of a filter. In this case, the chromatic dispersion of the fiber link acts as a phase filter that, together with the DML chirp, leads to some PM-to-IM conversion with an amplitude response showing a reduced 3 dB bandwidth, i.e., 1.2 GHz. Indeed, the first sinusoidal term in (11) leads to signal

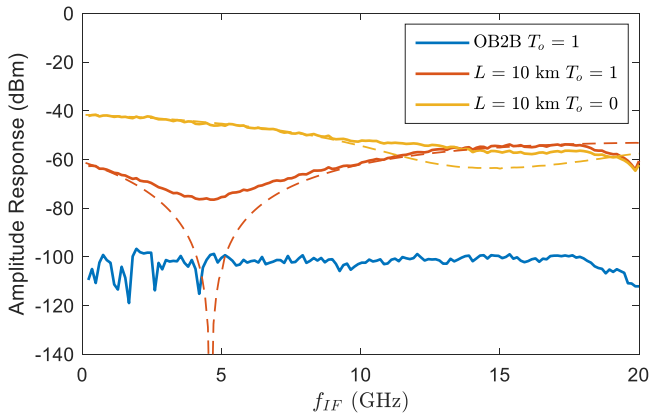

Fig. 3. Electrical frequency response at the mmW band ($f_{mmW} = 2f_{RF} - f_{IF}$) for OB2B and 10 km SSMF link without a filter ($T_o = 1$), and for 10 km fiber link using a 20 GHz bandwidth OBRF ($T_o = 0$).

cancellation around $f_{IF} = 4$ GHz due to dispersion effects when n = 1 in (13).

However, the frequency response of the complete system including both the DML chirp and fiber dispersion with the OBRF shows signal transmission along the entire frequency band since the first null is not held in the measured frequency range. Moreover, the 3 dB bandwidth now increases up to 4 GHz, which is slightly lower than the DML bandwidth. Note that the inclusion of the optical filtering stage leads to an effective gain of 20.5 dB at low frequencies due to the avoidance of the limiting factor $\sin^2\theta$ described in (11). Here, we observe the advantage of combining optical filtering and fiber dispersion to optimize the PM-to-IM up-conversion at the mmW band.

Fig. 3 includes the theoretical curves calculated from the analytical expressions included in Table I. A good agreement is found between theoretical and experimental results in spite of the particular features of the employed components in the experimental setup.

III. Experimental Transmission Measurements

A. System Performance

In this section, the system performance is analyzed when a signal at $f_{mmW} = 2f_{RF} \pm f_{IF}$ is photonically generated using a local oscillator operating at $f_{RF} = 20$ GHz, where f_{IF} is changed to transmit data at different mmW frequency bands. Additionally, the electrical power P_{RF} of the local oscillator was set to 23 dBm. For testing purposes, we employed a 25 MHz bandwidth QPSK signal using a root-raised-cosine filter with a 0.22 roll-off factor at various f_{IF} generated by DG, as shown in Fig. 1, that also allows to control the electrical power, P_{IF}, injected into the DML.

Fig. 4 displays the measured error-vector-magnitude (EVM) for different P_{IF} values after demodulating the transmitted data at several mmW bands. Concretely, each curve corresponds to the measurements carried out at 21, 26, 31, 35 and 39.8 GHz-bands over 10 km SSMF link which correspond to the

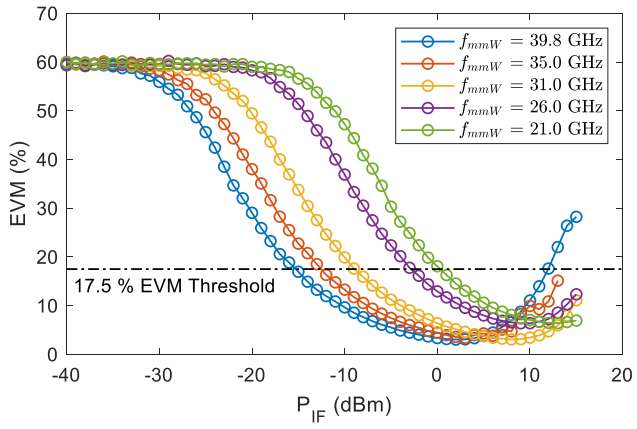

Fig. 4. Measured EVM vs P_{IF} at different generated mmW bands for 10 km SSMF link.

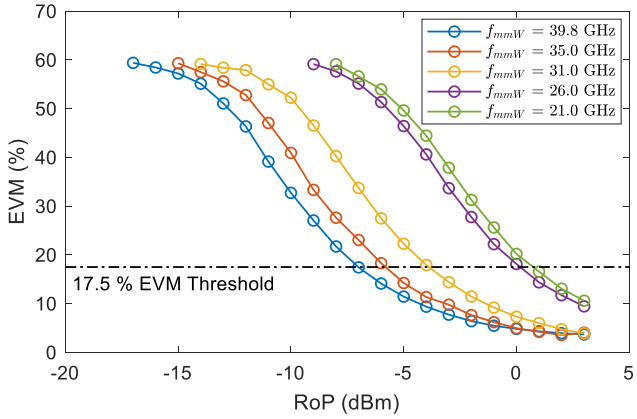

Fig. 5. Measured EVM vs RoP at different generated mmW frequencies for 10 km SSMF link.

f_{IF} values of 19, 14, 9, 5 and 0.2 GHz, respectively. Note that the EVM threshold of 17.5% for QPSK [19] is also plotted to ease the evaluation of the signal quality. As observed, the degradation of the signal is determined by the RF noise level at low operating P_{IF} levels, since the EVM is inversely proportional to the signal-to-noise ratio (SNR) in decibels (dBs) [20]. The EVM performance slowly degenerates with the decrease of the operation mmW frequency, i.e., f_{IF} increase, according to the uniform frequency decrease shown by the system transfer function displayed in Fig. 3. Indeed, the EVM values decrease with the increase of the electrical power P_{IF} up to a certain value where the system nonlinearities start to affect the quality of the recovered signal. That occurs at high operating power levels due to the number of intermodulation products and electrical subcarriers falling within the signal frequency band [21], [22].

In the following, the electrical operating power P_{IF} was set to 5 dBm to avoid the effects of the system nonlinearities. Fig. 5 shows the measured EVM performance for the previously selected f_{IF} values versus different RoP levels ranging from -17 to 3 dBm. As expected, the quality of the collected data again degenerates with the increase of f_{IF}. The deterioration of the recovered signal is only defined now by the detector noise at low RoP levels. Furthermore, EVM values are achieved below the 17.5% threshold from 21 up to 39.8 GHz for RoP levels larger than 0.7 and -7 dBm, respectively.

For the sake of completeness, Fig. 6 displays the measured EVM values for different received electrical power (ReP) levels under different scenarios. Concretely, Fig. 6(a)–(c) correspond to EVM measurements for $f_{mmW} = 39.8$, 31.0 and 29.0 GHz, i.e., when f_{IF} is set to 0.2, 9 and 19 GHz, respectively. Besides, EB2B is included for each f_{mmW}.

On one hand, the squares-curve has been obtained similarly to Fig. 4 by setting a fixed RoP = 3 dBm while P_{IF} was varied to obtain different ReP values depicted in X-axis. In Fig. 6(a), we can observe that EVM improves when ReP increases with P_{IF} up to values close to -33 dBm when the EVM lead to a U-shaped pattern because the link performance is affected by the system nonlinearities. In fact, the reason for the multi-valued curve characteristic is that lower ReP values are achieved for furtherly increased P_{IF}. This U-shaped behavior is also observed in Fig. 6(b) and (c) obtained at f_{mmW} of 31 and 21 GHz, respectively, although not as pronounced as in Fig. 6(a), where the maximum ReP value that can be achieved without distortion is higher. Note that the amplitude response is reduced for higher f_{IF}, i.e., lower f_{mmW}, as shown in Fig. 3.

On the other hand, the circles-curve was obtained when the RoP level was modified by adjusting the insertion losses (IL) in the VOA with a fixed P_{IF} = 5 dBm, as performed in Fig. 5. Such P_{IF} value ensures small signal regime operation, so nonlinear distortions are non-relevant in this case. Indeed, the curve overlapping with EB2B results demonstrates that the quality of the recovered upconverted signal is unrelated to the transmission system scheme. Therefore, we guarantee the transparency of the up-conversion photonic link for ReP values where system linearity is satisfied.

As an example, insets of Fig. 6(a)–(c) show the measured constellations for 10 km SSMF link at the corresponding generated bands of 39.8, 31 and 21 GHz for an electrical power P_{IF} of 5 dBm and an RoP of 3 dBm which measured ReP is -34.7, -43.82 and -51.84 dBm, respectively, according to the amplitude response in Fig. 3. In this case, the EVM values were 3.7, 3.9 and 10.7%, respectively. Note that, at these frequencies, the 17.5% EVM threshold is reached for ReP levels of -55.9, -57.1 and -57.0 dBm, respectively.

All experimental transmission results were performed by using QPSK signals without loss of generality because this modulation format permits a large operation power range that allows to observe distortion. However, different modulation formats have been considered in Fig. 7 for the sake of validation. As expected, note that similar results are obtained at 38 GHz for QPSK, 16-QAM, 32-QAM and 64-QAM for an EVM value of around 4% when RoP = 3 dBm and P_{IF} = 5 dBm.

B. Comparison With PM and IM

For the sake of final assessment, in this section we provide the comparison between two photonic mmW generation approaches based on PM and IM. In this case, the IM was implemented using a dual drive (DD-)MZM (Sumitomo T.DEH1.5) with 6 dB

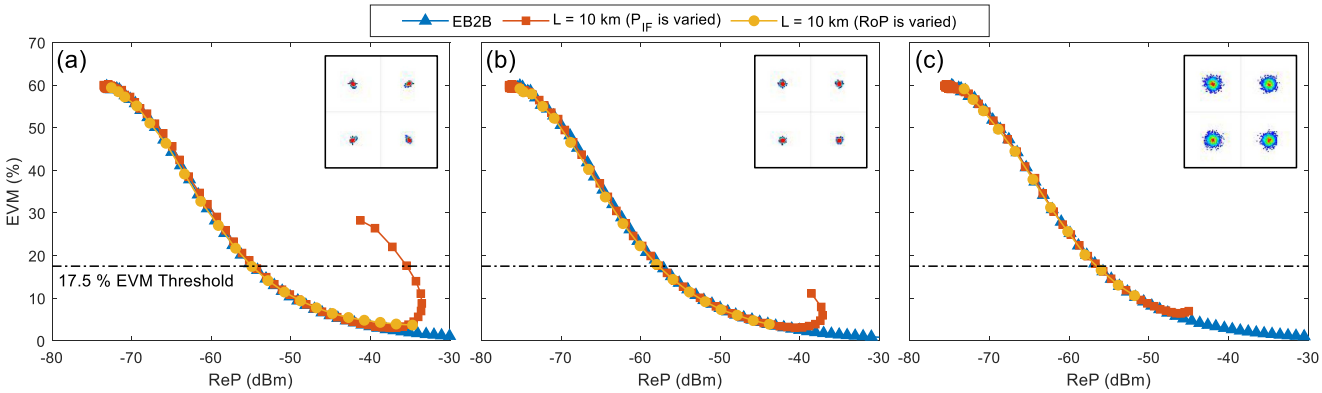

Fig. 6. Experimental EVM vs ReP levels for EB2B (▲) and when $L = 10$ km is considered by modifying data power P_{IF} (■) and RoP (•) and measured at different f_{mmW} values of (a) 39.8 GHz, (b) 31.0 GHz and (c) 21.0 GHz. Insets: measured QPSK constellations for 10 km SSMF link with a P_{IF} of 5 dBm and an RoP of 3 dBm.

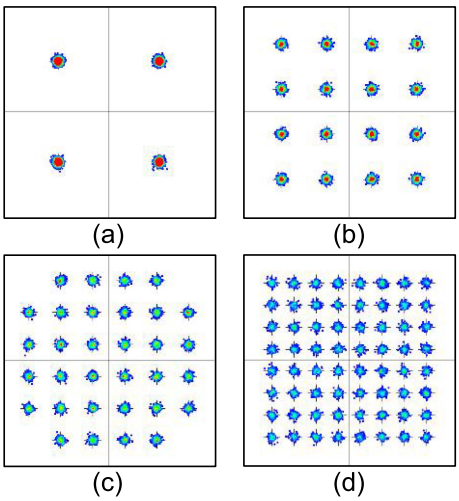

Fig. 7. Measured constellation when *RoP* $= 3$ dBm and $P_{IF} = 5$ dBm for different modulation formats (a) QPSK, (b) 16-QAM, (c), 32-QAM, and (d) 64-QAM at 38 GHz.

insertion losses, a 30 GHz 3dB-bandwidth and $V_\pi = 5.5\,V$. Note the former requires optical filtering to achieve optical carrier suppression, while an efficient biasing control is needed in the latter. In order to properly compare both configurations, both RoP and P_{IF} were ser to 0 dBm over 10 km SSMF link.

The optical spectra measured at P4 for PM and IM up-conversion are shown in Fig. 8(a). Two main differences can be observed with regards to the ER and the harmonic distortion (HD) obtained with each modulator. On one hand, the PM approach leads to 6 dB higher ER than using IM up-conversion, i.e., 20.3 dB. As is well known, the ER for IM is experimentally limited by the interferometric structure and the stability of the modulator. Indeed, ER higher than 20 dB requires the use of an external RF hybrid to drive the DD-MZM in order to avoid any unbalance on the amplitudes and phases between the modulating signals of both arms.

On the other hand, a clear difference is observed with regards to the third harmonic located at $3f_{RF}$. IM approach leads to

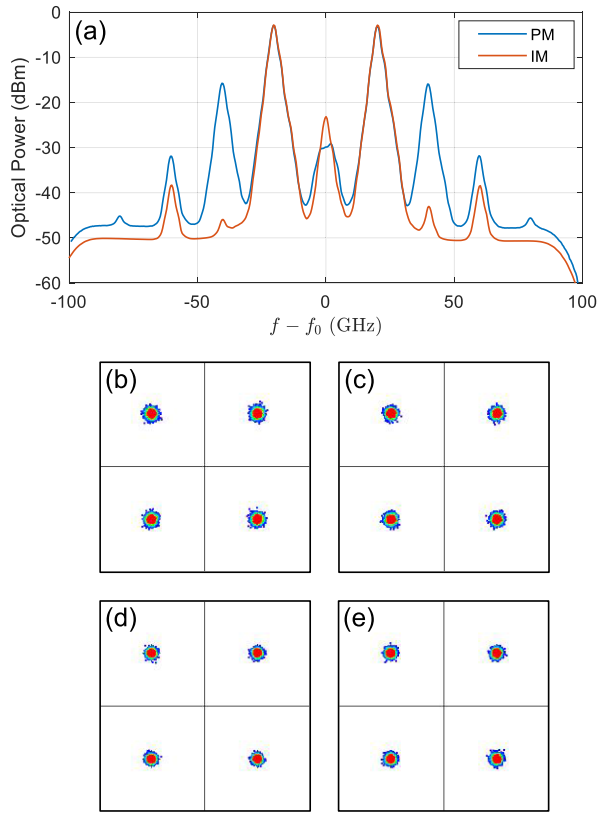

Fig. 8. (a) Experimental optical spectra at the PD input for optical up-conversion using PM and IM. Measured QPSK constellations for optical up-conversion using PM (b) in the lower band at 38 GHz and (c) the upper band 42 GHz whereas (d) and (e) correspond to lower and upper mmW band for optical up-conversion using IM, when RoP is set to 0 dBm and ReP is close to -44 dBm.

minimizing all odd-order harmonics when biasing voltage is controlled to suppress the optical carrier. However, although odd-order HD terms are present under PM scheme, the quality of the recovered data at lower (38 GHz) and upper (42 GHz) mmW bands are similar to those obtained in IM as shown in the constellation diagrams of Fig. 8. Therefore, we can conclude

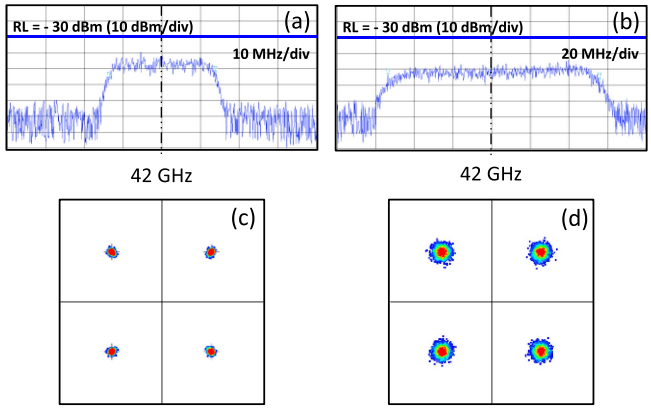

Fig. 9. Transmission of QPSK signal with different bandwidths with RoP = 3 dBm. Electrical spectra for upper mmW signal at 42 GHz with (a) 25 and (b) 100 MHz bandwidths and corresponding constellation diagrams in (c) and (d).

that, for PM up-conversion, the filtering requirements are not very stringent because the higher-order HD contribution is not significant.

Finally, note that similar RoP under both approaches leads to a 3dB optical noise floor difference due to the higher amplification level required in the PM setup. This is due to the reduced modulation efficiency and PM bandwidth used in the experimental setup, although its insertion losses are lower than for IM. Despite this experimental drawback, similar EVM values close to 4% with an ReP around -44 dBm are obtained in both setups for lower and upper mmW bands. Therefore, similar performance in both PM and IM solutions is assessed when optical losses are compensated by means of optical amplification to keep constant RoP with high stability in the PM case since any DC bias is required.

So far, in this section all experimental transmission results have been performed by using a 25 MHz QPSK signal due to the large operation power range below the corresponding EVM threshold. However, Fig. 9(a) and (b) show the electrical spectra for the upper mmW signal when the transmission bandwidth is set to 25 and 100 MHz QPSK, respectively. Note the different SNR shown in the electrical spectra, i.e., 30 and 22 dB for 25 and 100 MHz, respectively, lead to a different minimum EVM achieved in both cases. Indeed, the corresponding constellations diagrams are depicted in Fig. 9(c) and (d) where a minimum EVM of 3 and 8% was obtained when RoP = 3 dBm for 25 and 100 MHz, respectively.

IV. Conclusion

The use of a DML is proposed over a PM-assisted mmW signal generation system, where an optical filter is employed to provide PM-to-IM conversion together with the dispersive fiber link. Both comprehensive theoretical analysis and measurements of the system frequency response are provided showing very good agreement. A 25 MHz QPSK signal is employed for the purpose of testing the system transmission at different operating mmW frequencies, i.e., 21-39.8 GHz, under different setting parameters, RoP and P_{IF}, in a 10 km SSMF link, while system validation over 16- to 64-QAM is also presented. Both the system noise and the DML nonlinearities are shown to have a significant impact on the system performance and accordingly, the operation parameters range where our approach does not lead to any degradation with respect to EB2B data signals is defined.

The combination of optical filtering with fiber dispersion improves considerably the PM-to-IM up-conversion at the mmW band, as shown in our experimental setup, where 20 dB mmW gain is demonstrated.

Considering that PM optical losses are low compared to IM, our approach does not require extra electrical amplification since the SNR is not committed, and consequently, the EVM. A comparison with IM technique for mmW signal generation leads to assess the robustness of PM against dc-bias drifting allowing the avoidance of any external controller to stabilize the transmission. Note the simplicity of the PM approach, which does not require any RF hybrid component while employs an off-the-shelf optical filter with not very demanding characteristics.

Finally, while most of the previous PM approaches are based on fixed optical filtering that limits the mmW frequency operation, our proposal shows robustness and reconfigurability due to the intrinsic properties of the optical filtering stage. Additionally, it is commercially available and highly compatible with DWDM access networks by using multiport optical filtering, also shows a large scalability compared to nonlinear proposals. In this sense, our approach is very promising for the future deployment of energy efficient networks based on resource sharing and low consumption.

References

[1] W. Jiang, B. Han, M. A. Habibi, and H. D. Schotten, "The road towards 6G: A comprehensive survey," *IEEE Open J. Commun. Soc.*, vol. 2, pp. 334–366, 2021.

[2] X. Wang et al., "Millimeter wave communication: A comprehensive survey," *IEEE Commun. Surveys Tut.*, vol. 20, no. 3, pp. 1616–1653, Thirdquarter 2018.

[3] J. Yao, "Microwave photonics," *J. Lightw. Technol.*, vol. 27, no. 3, pp. 314–335, Feb. 2009.

[4] L. Vallejo, B. Ortega, J. Bohata, S. Zvanovec, and V. Almenar, "Experimental photonic 40–90 GHz millimetre-wave signal generation and 10 gb/s 32-QAM signal transmission over hybrid Fiber/FSO 5G networks," in *Proc. Int. Conf. Transp. Opt. Netw.*, 2019, pp. 1–4.

[5] H. Chi, X. Zou, and J. Yao, "Analytical models for phase-modulation-based microwave photonic systems with phase modulation to intensity modulation conversion using a dispersive device," *J. Lightw. Technol.*, vol. 27, no. 5, pp. 511–521, Mar. 2009.

[6] G. Qi, J. Yao, J. Seregelyi, S. Paquet, and C. Belisle, "Optical generation and distribution of continuously tunable millimeter-wave signals using an optical phase modulator," *J. Lightw. Technol.*, vol. 23, no. 9, pp. 2687–2695, Sep. 2005.

[7] P. Shen, J. James, N. J. Gomes, P. G. Huggard, and B. N. Ellison, "Low-cost, continuously tunable, millimeter-wave photonic LO generation using optical phase modulation and DWDM filters," *IEEE Photon. Technol. Lett.*, vol. 20, no. 23, pp. 1986–1988, Dec. 2008.

[8] B. Chen, S. Zheng, H. Chi, X. Zhang, and X. Jin, "An optical millimeter-wave generation technique based on phase modulation and Brillouin-assisted notch-filtering," *IEEE Photon. Technol. Lett.*, vol. 20, no. 24, pp. 2057–2059, Dec. 2008.

[9] X.-H. Huang, C.-Y. Li, H.-H. Lu, C.-R. Chou, H.-M. Hsia, and Y.-H. Chen, "A bidirectional FSO communication employing phase modulation scheme and remotely injection-locked DFB LD," *J. Lightw. Technol.*, vol. 38, no. 21, pp. 5883–5892, Nov. 2020.

[10] P. T. Dat et al., "Millimeter-wave radio-over-fiber system using optical phase modulation and photonic downconversion for uplink fronthaul transmission," *Opt. Lett.*, vol. 46, no. 10, pp. 2493–2496, 2021.

[11] H.-H. Lu et al., "Two-way 5G NR Fiber-wireless systems using single-carrier optical modulation for downstream and phase modulation scheme for upstream," *J. Lightw. Technol.*, vol. 41, no. 6, pp. 1749–1758, Mar. 2023.
[12] C.-Y. Li et al., "A flexible two-way PM-based Fiber-FSO convergence system," *IEEE Photon. J.*, vol. 10, no. 2, Apr. 2018, Art. no. 7901509.
[13] X. Li, J. Xiao, and J. Yu, "W-band vector millimeter-wave signal generation based on phase modulator with photonic frequency quadrupling and precoding," *J. Lightw. Technol.*, vol. 35, no. 13, pp. 2548–2558, Jul. 2017.
[14] L. Zhao, J. Yu, L. Chen, P. Min, J. Li, and R. Wang, "16QAM Vector millimeter-wave signal generation based on phase modulator with photonic frequency doubling and precoding," *IEEE Photon. J.*, vol. 8, no. 2, Apr. 2016, Art. no. 5500708.
[15] L. Vallejo et al., "On the 40 GHz remote versus local photonic generation for DML-based C-RAN optical fronthaul," *J. Lightw. Technol.*, vol. 39, no. 21, pp. 6712–6723, Nov. 2021.
[16] L. A. Neto et al., "Simple estimation of fiber dispersion and laser chirp parameters using the downhill simplex fitting algorithm," *J. Lightw. Technol.*, vol. 31, no. 2, pp. 334–342, Jan. 2013.
[17] I. P. Kaminow, T. Li, and A. E. Willner, *Optical Fiber Telecommunications Volume VIB, Sixth Edition: Systems and Networks*. 6th ed., Cambridge, MA, USA: Academic, 2013.
[18] J. P. Yao, G. Maury, Y. L. Guennec, and B. Cabon, "All-optical subcarrier frequency conversion using an electrooptic phase modulator," *IEEE Photon. Technol. Lett.*, vol. 17, no. 11, pp. 2427–2429, Nov. 2005.
[19] ETSI, "5G; NR; User Equipment (UE) radio transmission and reception; Part 2: Range 2 standalone, 3GPP, Sophia Antipolis, France, Tech. Specification 38.101-2 version 15.7.0 Release 15," 2019.
[20] N. Argyris et al., "A 5G mmWave Fiber-wireless IFoF analog mobile fronthaul link with up to 24-gb/s multiband wireless capacity," *J. Lightw. Technol.*, vol. 37, no. 12, pp. 2883–2891, Jun. 2019.
[21] C. Lim, A. Nirmalathas, K.-L. Lee, D. Novak, and R. Waterhouse, "Intermodulation distortion improvement for Fiber–Radio applications incorporating OSSB+C modulation in an optical integrated-access environment," *J. Lightw. Technol.*, vol. 25, no. 6, pp. 1602–1612, Jun. 2007.
[22] J. Wang, C. Liu, M. Zhu, A. Yi, and G.-K. Chang, "Closed-form analysis of intra/inter-band cross-modulation in multiband radio-over-fiber systems," in *Proc. IEEE Glob. Commun. Conf.*, 2013, pp. 2454–2460.

M. Botella-Campos received the B.Sc. degree in telecommunications systems, sound and image engineering and the M.Sc. degree in telecommunication technologies, systems and networks in 2019 and 2021, respectively, from Univertat Politècnica de València (UPV), Valencia, Spain, where she is currently working toward the Ph.D. degree in telecommunication engineering program. In 2021, she joined Instituto de Telecomunicaciones y Aplicaciones Multimedia, Photonic Research Labs, UPV. Her research interests include microwave photonics, mmW generation, as well as RoF/FSO for 5G and beyond, and optical networks.

J. Mora received the M.Sc. degree in physical sciences and the Ph.D. degree in physics from the Universitat de València, Valencia, Spain, in 1999 and 2005, respectively. From 1999 to 2004, he was with the Department on Applied Physics, Universitat de València. Since 2004, he has been a Senior Researcher with the Photonics Research Labs, Institute of Telecomunications and Multimedia (ITEAM), Universitat Politècnica de València, Valencia, Spain. He has collaborated in many regional, national and international R&D projects involving research and industry. He was the Co-Founder of the UPV spin-off company EPHOOX in 2016, specialized on advanced instrumentation for Microwave Photonics and Radio over Fiber systems. He has an H-factor of 25. He has authored or coauthored more than 100 papers and conference contributions covering a wide range of fields using photonic technology (fibre bragg gratings for sensing applications, optical signal processing, microwave photonics, reconfigurable and convergent optical for wired/wireless services and quantum cryptography). He was the recipient of the Extraordinary Doctorate Prize of the Universitat de València in 2006.

B. Ortega (Senior Member, IEEE) received the M.Sc. degree in physics from the Universidad de Valencia, Valencia, Spain, in 1995, and the Ph.D. degree in telecommunications engineering from the Universidad Politécnica de Valencia, Valencia, in 1999. She is currently with the Departamento de Comunicaciones, Universitat Politècnica de València, where she has been a Full Professor since 2009. She has collaborates as a Group Leader with the Photonics Research Labs, Institute of Telecommunications and Multimedia Applications. She has authored or coauthored more than 200 papers and conference contributions in fibre Bragg gratings, microwave photonics, and optical networks. She has got several patents and is also a Co-Founder of EPHOOX company. Her research interests include optical devices, optical networks, and microwave photonic systems and applications. She has participated in a large number of European Networks of Excellence and R&D projects and other national ones.